ELECTRONICS RESEARCH CENTER

NATIONAL AERONAUTICS AND SPACE ADMINISTRATION

PM-82

ON THE USE
OF HODOGRAPHIC MAPPING
IN TRAJECTORY ANALYSIS

By Fang Toh Sun
Electronics Research Center
Cambridge, Massachusetts 02139

June 1969

NATIONAL AERONAUTICS AND SPACE ADMINISTRATION

ABSTRACT

The classic method of hodographic mapping and its modern developments are reviewed, and their applications to the analysis of trajectory problems in space-flight are discussed. The bacis concepts and principles of the hodographic mapping, as originated by Möbius and Hamilton, are formulated on a broad basis in the language of differential geometry. Applications of these fundamental formulas to a general force field, an arbitrary central force field, and an inverse-square field are successively presented; and the Hamiltonian circular hodograph and its polar version, briefly reviewed. The concepts and methods of normalized hodographic mapping, and constraining hodograph, and the osculating hodograph are introduced, and their applications in specific classes of trajectory problems are concisely discussed. Hodographs for Kepler orbits in rotating coordinates are introduced and illustrated with the view of aiding the comparison of the restricted three-body orbits with the two-body orbits. While the main concern of this survey is the velocity hodograph, a short introduction on its extension to other state spaces is included. As final remarks, the hodograph method of trajectory analysis is briefly compared with the classical analytic methods in Hamiltonian mechanics.

INTRODUCTION

The method of hodographic mapping, as originated by Möbius (ref.1) and Hamilton (refs. 2,3) in the 1840's was primarily for the study of the motion of celestial bodies. Such a mapping has later found its applications in gasdynamics, especially in problems of supersonic flow; but, ironically speaking, it has been practically ignored in Celestial Mechanics, even in the realm of Kepler motion, where Hamilton's circular hodograph has its immediate and elegant applications. Recent

studies* show that the method of hodographic mapping not only proves to be a powerful method in dealing with Kepler motion, but also helpful in many problems of modern astrodynamics in connection with space flight. In the following, Möbius and Hamilton's original concepts will be formulated in modern terms on a broad basis so as to form the foundations for later applications to Keplerian as well as non-Keplerian motions. The Hamiltonian hodograph and its polar version will be briefly reviewed, and several new concepts and methods of hodographic mapping for the analyses of various classes of current trajectory problems will be introduced and discussed.

BASIC CONCEPTS AND FORMULATION IN HODOGRAPHIC MAPPING

Consider the motion of a mass particle of mass m in a general force field. At each instant, there is a velocity vector $\vec{V}$ associated with a position vector $\vec{r}$. The path described by the tip of $\vec{r}$ in the position space, or the $\vec{r}$-space, is generally referred to as the trajectory, and that described by the tip of $\vec{V}$ in the velocity space, or the $\vec{V}$-space, is the hodograph of the motion, as called by Möbius (ref.1) and Hamilton (ref. 2). From a broader point of view, a hodograph, or, more precisely, the velocity hodograph, may be regarded as the trajectory in the $\vec{V}$-space, or the $\vec{V}$-trajectory, while that in the $\vec{r}$-space, the $\vec{r}$-trajectory. Although a motion is usually represented by its $\vec{r}$-trajectory, it can be represented equally well, or even better, by its $\vec{V}$-trajectory, as the latter may possess a simpler geometry then its counterpart in the $\vec{r}$-space. This is particularly obvious, as it will be seen later, in the case of Kepler motion.

In a definitive motion, the correspondence between $\vec{r}$ and $\vec{V}$ is one-to-one. Such a correspondence may be viewed as a mapping, and the $\vec{V}$-trajectory may be viewed as the hodograph image of the $\vec{r}$-trajectory. The latter is generally a space curve in the three-dimensional $\vec{r}$-space,

*See, e.g., refs. 5-7, 9-12, 19-22, etc.

and so is the former in the three-dimensional $\vec{V}$-space (Fig. 1). The geometrics of the two curves are closely related through the dynamics of the motion. Table I is a summary of the essential relations pertaining to each of the two vector spaces, and their inter-relations which follow directly from the basic concepts, definitions, and standard formulas of differential geometry, and hold for any arbitrary force field.

TABLE I - BASIC FORMULAS

	$\vec{r}$-Trajectory	$\vec{V}$-Trajectory
Curvature	$\kappa = \frac{\lvert\vec{V}\times\vec{F}\rvert}{mV^3}$ (1a)	$K = \frac{m\lvert\vec{F}\times\dot{\vec{F}}\rvert}{F^3}$ (1b)
Torsion	$\tau = \frac{[\vec{V},\vec{F},\dot{\vec{F}}]}{\lvert\vec{V}\times\vec{F}\rvert^2}$ (2a)	$\zeta = \frac{m[\vec{F},\dot{\vec{F}},\ddot{\vec{F}}]}{\lvert\vec{F}\times\dot{\vec{F}}\rvert^2}$ (2b)
Frenet Triad		
Unit Tangent	$\vec{e}_t = \frac{\vec{V}}{V}$ (3a)	$\vec{e}_T = \frac{\vec{F}}{F}$ (3b)
Unit Principal Normal	$\vec{e}_n = \frac{(\vec{V}\times\vec{F})\times\vec{V}}{\lvert\vec{V}\times\vec{F}\rvert V}$ (4a)	$\vec{e}_N = \frac{(\vec{F}\times\dot{\vec{F}})\times\vec{F}}{\lvert\vec{F}\times\dot{\vec{F}}\rvert F}$ (4b)
Unit Binormal	$\vec{e}_b = \frac{\vec{V}\times\vec{F}}{\lvert\vec{V}\times\vec{F}\rvert}$ (5a)	$\vec{e}_B = \frac{\vec{F}\times\dot{\vec{F}}}{\lvert\vec{F}\times\dot{\vec{F}}\rvert}$ (5b)
Angular Velocity of Rotation	$\vec{\omega} = V(\tau\vec{e}_t+\kappa\vec{e}_b)$ (6a)	$\vec{\Omega} = \frac{F}{m}(\zeta\vec{e}_T+K\vec{e}_B)$ (6b)
Inter-relations	$\vec{V} = \dot{\vec{r}}, \quad \vec{F} = m\dot{\vec{V}}$ (7)	
	$\vec{e}_T = \frac{m}{F}(\dot{V}\vec{e}_t+\kappa V^2\vec{e}_n)$ (8)	
	$\frac{d\xi}{ds} = \frac{F}{V}$ (9)	

$(\dot{}) \equiv \frac{d}{dt}(\ )$

This set of formulas is by no means comprehensive, but it shows clearly that the intrinsic geometric properties of the trajectories in the $\vec{r}$- and $\vec{V}$-spaces are determined by the force field $\vec{F}$, and, conversely,

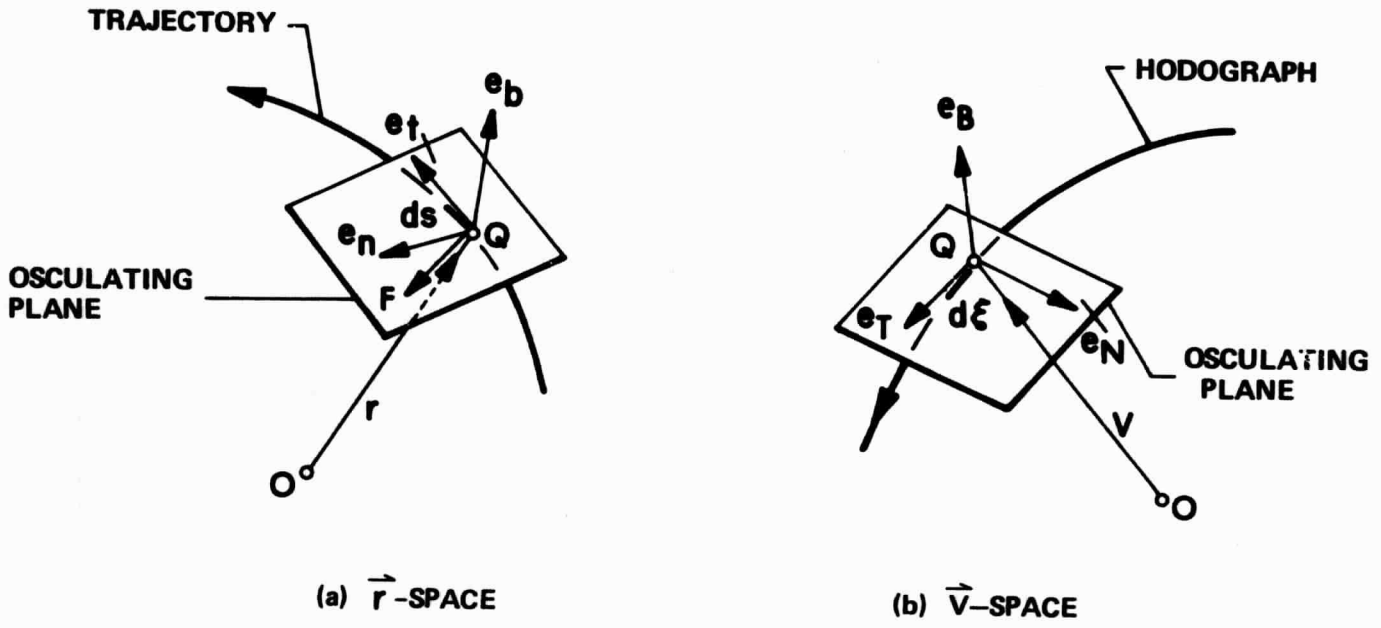

Figure 1.- Trajectory in the Position and Velocity Spaces: General Force Field

the nature of the force field and the dynamics of motion are manifested through these intrinsic properties of the $\vec{r}$- and $\vec{V}$-trajectories. It also shows how the trajectory geometries in the two vector spaces are interlocked; and in particular, it reveals the following features characterizing a hodographic mapping in general, as contained in Hamilton's original exposition:[2]

(1) At corresponding points, the tangent vector of the $\vec{r}$-trajectory is always parallel to the radius vector to the $\vec{V}$-trajectory; and the tangent vector to the $\vec{V}$-trajectory is always parallel to the resultant force vector (Eqs. (3a,b)).

(2) The magnitude of the force is to the instantaneous speed of motion as the line element $d\xi$ of the $\vec{V}$-trajectory is to the corresponding element ds of the $\vec{r}$-trajectory (Eq. (9)).

As an additional observation, Eq. (8) shows that the resultant force vector is in the osculating plane of the $\vec{r}$-trajectory.

So far, nothing has been specified for the force field. Now, consider a central force field

$$\vec{F}(\vec{r}) = f(r)\ \vec{e}_r \tag{10}$$

where f(r) is an arbitrary scalar function of r, and the origin is at the force center. The motion in such a field is well known to be characterized by the presence of a constant angular momentum vector,

$$\vec{h} = \vec{r} \times \vec{V} \tag{11}$$

Hence, the motion is planar, and the trajectories in $\vec{r}$- and $\vec{V}$-spaces are both plane curves. For such a field, most relations in Table I can be simplified. In particular, we note that Eqs. (1,2,5,6) reduce to

$$\kappa = h|f|mrV^3 \tag{12a}$$

$$K = mh/r^2|f| \tag{12b}$$

$$\tau = T = 0 \tag{13}$$

$$\vec{e}_b = \vec{e}_B = \vec{h}/h \equiv \vec{e}_h \tag{14}$$

$$\vec{\omega} = |f|\vec{h}/mrV^2 \tag{15a}$$

$$\vec{\Omega} = \vec{h}/r^2 \tag{15b}$$

In addition, the following inter-relations hold:

$$\vec{e}_T = \pm\vec{e}_r, \quad \vec{e}_N = \pm\vec{e}_\theta \tag{16}$$

where the + sign is to be taken when the force is repulsive (f>0), and the - sign, when it is attractive (f<0). Note here the unit vector triad $(\vec{e}_r,\vec{e}_\theta,\vec{e}_h)$ is the usual polar reference frame for the $\vec{r}$-trajectory. Eqs. (13,16) show that in any central force field the local Frenet frame $(\vec{e}_T,\vec{e}_N,\vec{e}_B)$ for the $\vec{V}$-trajectory is identical to the local polar frame $(\vec{e}_r,\vec{e}_\theta,\vec{e}_h)$ for the $\vec{r}$-trajectory. Similarly, the local Frenet frame for the $\vec{r}$-trajectory is identical to the local polar frame for the $\vec{V}$-trajectory, both given by the triad $(\vec{e}_t,\vec{e}_n,\vec{e}_h)$. It follows that we may identify $\vec{\omega}$ as the angular velocity of $\vec{V}$; and $\vec{\Omega}$ as that of $\vec{r}$; and write in the usual notations,

$$\vec{\omega} = \beta\,\vec{e}_h \tag{17a}$$

$$\vec{\Omega} = \theta\,\vec{e}_h \tag{17b}$$

The vector geometry of the trajectories in the $\vec{r}$- and $\vec{V}$-planes are shown in Fig. 2.

A comparison of Eqs. (12a) and (12b) shows that the curvature formula for the $\vec{V}$-trajectory takes a simpler form than that for the r-trajectory; the latter depends on the orbital speed, but the former does not. By introducing the radii of curvature,

$$\rho = \frac{1}{\kappa}\ , \quad R = \frac{1}{K} \tag{18}$$

Eqs. (12a,b) yield the simple relation

$$\rho R = h\,\sec^3\phi \tag{19}$$

where ϕ is the path angle with reference to the local horizontal.

Now, if we further specify the field to be an inverse square one, i.e.,

$$f(r) = \pm\,\frac{m\mu}{r^2} \tag{20}$$

where μ is the gravitational constant, and the plus and minus signs indicate a repulsive field and an attractive field, respectively. Eqs. (12b,18) yield immediately

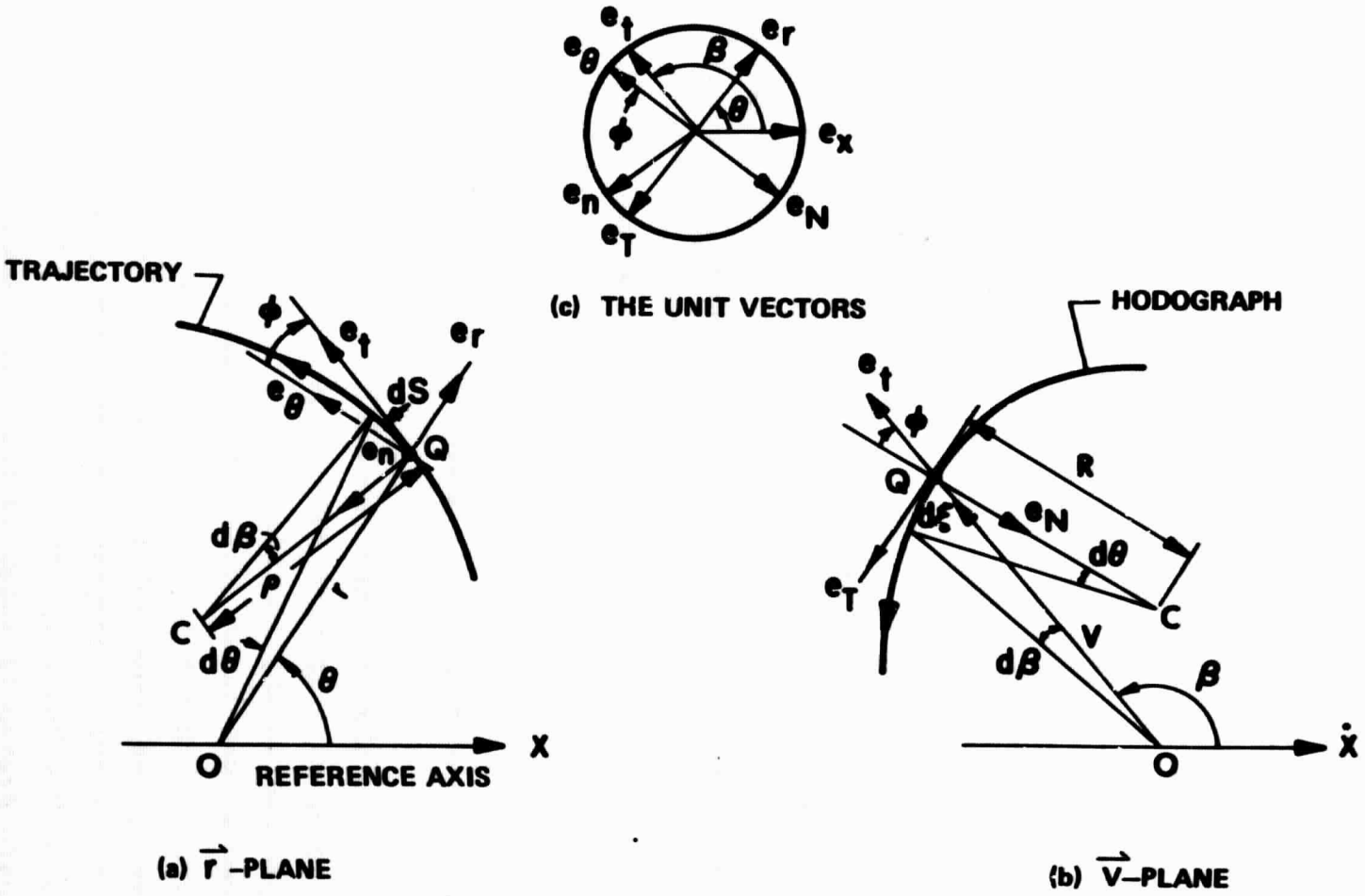

Figure 2.- Trajectory in the Position and Velocity Spaces: Central Force Field

$$R = \frac{\mu}{h} \tag{21}$$

Thus, the $\vec{V}$-trajectory is a circle, whose radius in a given inverse-square field, depends on the scalar angular momentum h only. This is Hamilton's Law of Circular Hodograph (ref. 2). It is interesting to note here that this law was proved without any knowledge of the $\vec{r}$-trajectory. On the contrary, Hamilton showed that the orbit was a conic by using his circular hodograph. Instead of his geometric proof, it can be easily seen here from Eq. (21), together with Eq. (19) to give

$$\rho = \frac{h^2}{\mu} \sec^3 \phi \tag{22}$$

which can be recognized at once as the radius of curvature of a conic. No doubt the hodograph representation serves as a much simpler description of the motion than its $\vec{r}$-trajectory, the orbit, in the case of an inverse-square field. The conclusions deduced so far hold for an attractive field as well as a repulsive one. However, in the following, particular attention will be focused on the attractive inverse-square field, or the Newtonian gravity field, which is the main concern in trajectory problems in space-flight, and it will be so assumed unless otherwise stated.

THE HAMILTONIAN CIRCULAR HODOGRAPH AND ITS POLAR VERSION

It is understood that the Hamiltonian circular hodograph was derived with reference to a frame fixed in the inertial space, and that it is to be expressed in any inertial velocity coordinate system. However, it has been proved later that in the non-inertial velocity coordinates, V_r and V_θ, in the local vertical and local horizontal directions respectively, the hodograph is still a circle (ref. 7). That is, Hamilton's Law of Circular Hodograph may be extended to the (V_r, V_θ) coordinate system. The hodograph of the absolute velocity described in this coordinate system is known as the polar hodograph.* The

*Formerly called "the special hodegraph" in ref. (7).

equation of the Hamiltonian circular hodograph in the inertial coordinates (V_x, V_y), where, the subscripts x and y refer to the apsidal and lateral directions of the orbital conic respectively, and that of the polar hodograph in the non-inertial coordinates (V_r, V_θ) may be put into the following forms:

$$V_x^2 + (V_y - C)^2 = R^2 \tag{23}$$

$$V_r^2 + (V_\theta - R)^2 = C^2 \tag{24}$$

with

$$R = \frac{\mu}{h} \ , \ C = \varepsilon \frac{\mu}{h} \tag{25}$$

where ε is the numerical eccentricity of the conic orbit. Eqs (23,24) show that either the Hamiltonian hodograph circle or its polar version may be specified by the two parameters R and C. However, it is to be noted that, in Hamiltonian hodograph, R is the radius of the hodograph circle, and C is the distance between its center and the origin; while, in the polar version, the roles of R and C are interchanged. For either version, Eq. (25) show that the numerical eccentricity of the orbital conic is given by

$$\varepsilon = C/R \tag{26}$$

Thus, we have

$C < R$: $\varepsilon < 1$, elliptic orbit
$C = R$: $\varepsilon = 1$, parabolic orbit
$C > R$: $\varepsilon > 1$, hyperbolic orbit

A circular orbit is a particular case of the elliptic orbit with $\varepsilon = 0$, corresponding to $C = 0$. So far it has been tacitly assumed that the angular momentum h is non-vanishing. In the limiting case of $h = 0$, we have $R \to \infty$, $C \to \infty$, and the $\vec{r}$- and $\vec{V}$-trajectories degenerate into the V_x- and V_r- axes, respectively. Such a degenerate case will be excluded unless otherwise stated. The geometry of the three main types of conic orbits and their corresponding Hamiltonian and polar hodographs are shown in Fig. 3. Their general correlations are graphically depicted in Fig. 4. Detailed correlations for each of the three types of a

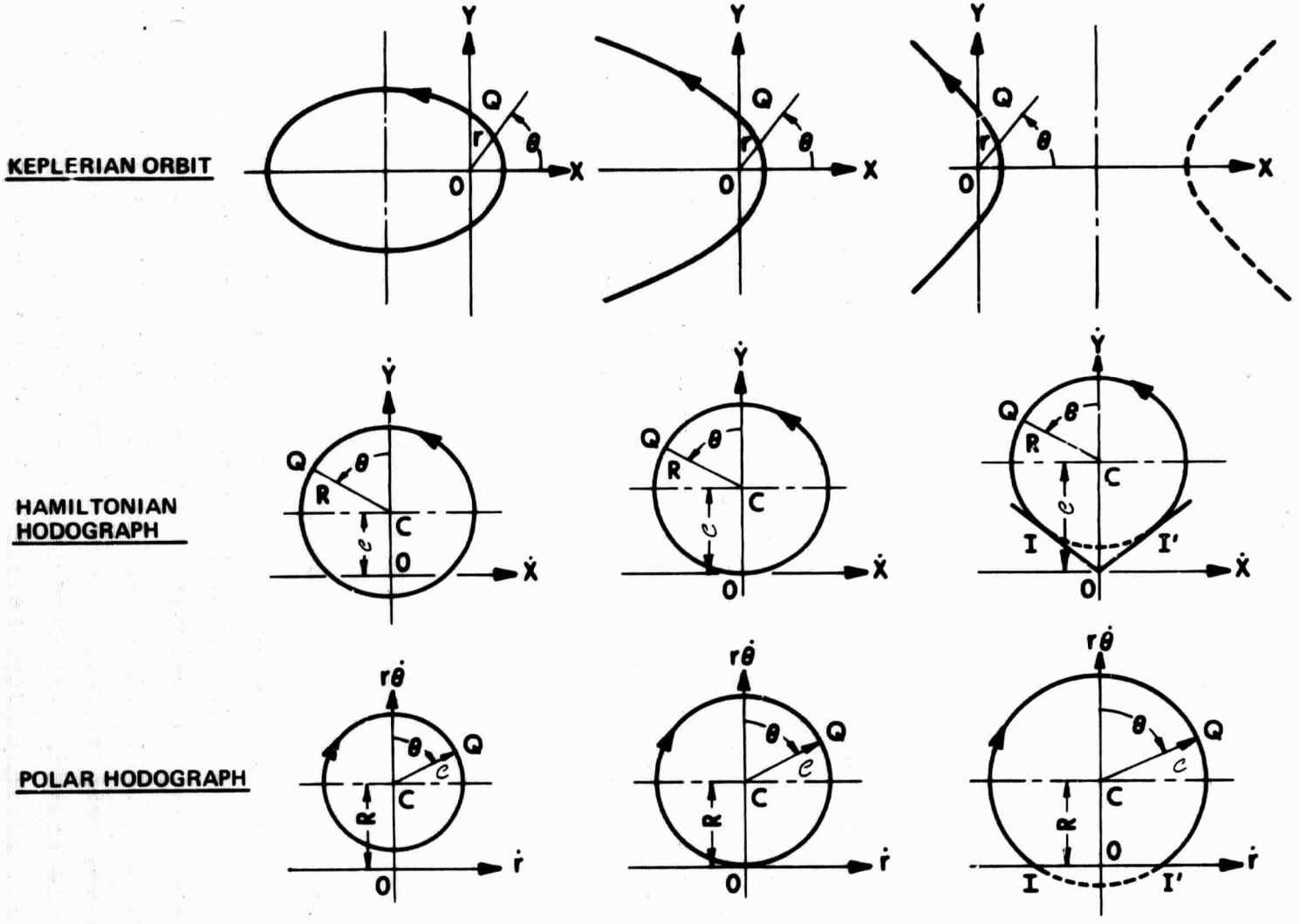

Figure 3.- The Keplerian Orbits and Their Hodograph Images

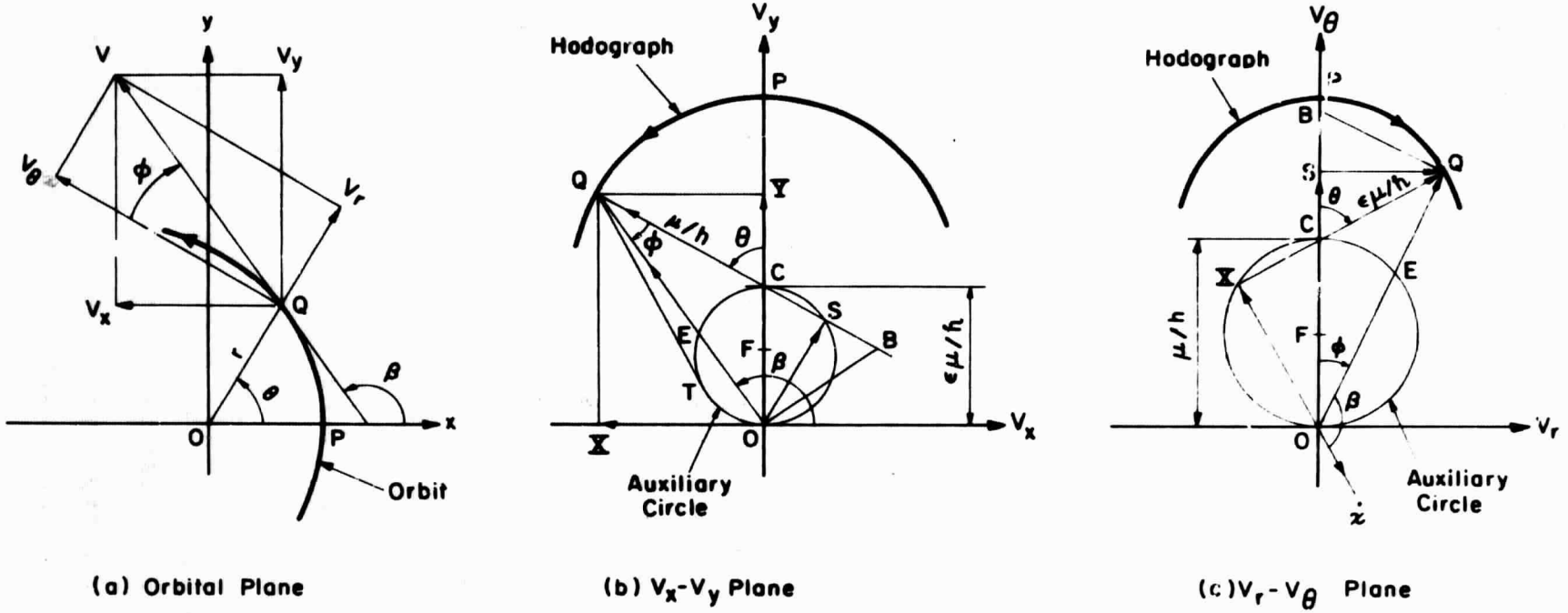

Figure 4.- General Correlation Between the Orbital Plane and the Hodograph Planes

conic orbit, the elliptic, the parabolic, and the hyperbolic, and the pertinent formulas are found in refs. 7 and 10. It should be mentioned that, for elliptic motion, one complete circuit along the hodograph circle corresponds to one complete circuit along the orbital ellipse; however, for hyperbolic motion, the hodograph circle is divided into two arcs, with the major arc corresponding to the motion along the near (field center) branch of the orbital hyperbola, which is the one realized in an attractive field, and the minor arc corresponding to its far branch, the one realized in a repulsive field; their junctions (points I, I' in Fig. 3) being the images of the points at infinity in the orbit plane. A parabolic orbit is the borderline between the elliptic and hyperbolic cases, its point at infinity being mapped into the origin of the hodograph. It should also be noted that all equations presented in the preceding section were formulated with reference to an inertial frame, and modifications or new interpretations are needed in applying them to the polar frame of reference. Such changes have been implied in Eq. (24), and Fig. 4(C), and they will not be elaborated here.

Based on these preliminaries, the main advantages of hodographic mapping in an inverse-square field may be summarized as follows:

(1) A conic orbit is mapped onto a circle, regardless of its numerical eccentricity, hence the mapping provides a unified approach to the treatment of orbits of various conic types, a treatment often sought by theoretical analysts.

(2) It also provides a unified approach to the dynamical analysis for an attractive field and a repulsive field. Thus its applications are not confined to space dynamics.

(3) Hodographic mapping enables one to replace the geometry of orbital conics by the geometry of circles, thus greatly simplifying the analysis. In particular, while it takes an infinite plane to describe a hyperbolic or parabolic orbit in the position space, it takes only a finite portion of the velocity plane to describe its hodograph.

All the foregoing remarks apply to both the Hamiltonian hodograph and its polar version. As noted earlier, the two versions of the

orbital hodograph may be converted to each other by merely interchanging the radius of the hodograph circle and its center-to-origin distance. Algebraically, in expressing orbital relations, the transformation from the inertial coordinates (V_x, V_y) to the non-inertial polar coordinates (V_r, V_θ) and vice versa may be effected simply by interchanging the two parameters R and C.

As a final remark, the mapping of orbital conics onto its hodograph circle may be viewed purely geometrically as a pedal transformation followed by inversion and proper rotation, as shown by Altman (ref. 20). It can be further proved that such an assertion not only holds for the conic orbit in an inverse-square field, but also for the orbits in any central force field.

Of the numerous applications of the circular hodograph, one elementary example will be cited. As the Hamiltonian (or the polar) hodograph implies, at any point on a conic orbit, we may write

$$\vec{V} = C\,\vec{e}_y + R\,\vec{e}_\theta \tag{27}$$

which shows that the velocity vector $\vec{V}$ may be resolved into the non-orthoginal components

$$\vec{V}_y = C\,\vec{e}_y\,, \quad \vec{V}_\theta = R\,\vec{e}_\theta \tag{28}$$

and the hodograph geometry indicates immediately that, as the point Q moves along the orbit, $\vec{V}$ changes continuously, but its component $\vec{V}_y$ remains fixed in magnitude as well as in direction in the inertial space, and $\vec{V}_\theta$ remains fixed in magnitude. They are the so-called invariant two-body velocity components (refs. 14, 15). A geometric proof in the orbital plane is given in the classic work of Whittaker (ref. 4). This remarkable theorem, as seen here, is a direct consequence of the circular hodograph. Obviously, it holds for all elliptic, parabolic, and hyperbolic orbits. This example illustrates clearly the power of hodographic mapping in dealing with conic orbits. A formal hodographic proof of this theorem is found in ref. (16). It will be further discussed later in connection with orbital perturbation problems. More examples of applications of the circular hodographs, ranging from elementary ones to more sophisticated ones, are found in

refs. (6, 7, 9, 10, etc.). In the following, further applications to advanced trajectory problems with extended and modified concepts and techniques of hodographic mapping will be introduced.

THE NORMALIZED HODOGRAPHIC MAPPING FOR FAMILIES OF KEPLERIAN TRAJECTORIES

A recent development in line with the Hamiltonian circular hodograph is the introduction of the non-dimensional velocity space, defined by

$$\vec{v} = \frac{h}{\mu} \vec{V} \tag{29}$$

for the motion in a Newtonian gravity field, h being the scalar angular momentum per unit orbiting mass. Eqs. (23) and (29) show that the Hamiltonian hodograph becomes a unit circle regardless of the size and shape of the conic orbit. Such a mapping will be referred to as the normalized hodographic mapping. It finds its special application in the analysis of families of Keplerian trajectories, which arise frequently in mission planning, orbit determination, trajectory optimization, and many other space-flight problems. Under such a mapping, distinct members of the family will be mapped onto distinct unit circles, if the origin of the $\vec{v}$-space is fixed, as we ordinarily do in the classical hodographic mapping. However, to further simplify the hodograph geometry, we will regard the center of the hodograph circle fixed, and let the hodograph origin vary. In this way, different Kepler orbits in the same plane will be mapped onto the same unit circle, but with different origins in the plane of this circle. Thus, corresponding to a family of Kepler orbits in the $\vec{r}$-space, we will have a set of origin points in the $\vec{v}$-space, the totality of which constitute the locus of origins, called the O-locus. The unit circle together with the O-locus constitute the hodograph image of the entire family. Under proper constraints, the O-locus of a coplanar family is a plane curve. For a spatial family, the unit hodograph circle generates a unit hodograph sphere, and the O-locus is usually a surafce in the $\vec{v}$-space. To further fix the idea, we will impose a condition that all members of the family to be treated pass through a common point fixed in the

$\vec{r}$-space, whatever other constraints may be present. Such a family in the $\vec{r}$-space and its hodograph image in the $\vec{v}$-space are graphically depicted in Fig. 5. At this point, several remarks are in order:

(1) The normalization of the velocity space as defined by Eq (29) differs from the usual normalization or non-dimensionalization in that the factor h/μ introduced is not an absolute constant regarding the whole family. While μ is constant in a given Newtonian field, h is constant only along each trajectory but it varies from one trajectory to another.

(2) While the ordinary hodographic mapping is a point-to-point transformation, the normalized one is essentially a curve-to-point transformation in the sense that corresponding to each trajectory in the $\vec{r}$-space there is a definite point on the O-locus. The converse is true under the present co-terminal condition, and the mapping is thus one-to-one (except possibly at certain singular points).

(3) While the O-locus defines the non-dimensional velocity vectors $\vec{v}$ for different trajectories on one hand, it also displays the eccentricity vectors ($\vec{\epsilon}$) on the other hand. It is in fact also the locus of the tip of the eccentricity vector* of the family.

As a consequence of these features (especially item No. 2), the normalized hodographic mapping enables one to deal with, instead of the infinitely many trajectories of the family, a unit circle and the O-locus only. The global characteristics of the family may then be observed from the geometry of the normalized hodograph image, and so are the characteristics of any particular trajectories of the family. Very often a trajectory family of complicated geometry in the $\vec{r}$-space has a strikingly simple image in the $\vec{v}$-space, and the analysis becomes a simple matter.

The concept of normalized hodographic mapping in an inertial velocity space was first introduced in ref. 10, and later applied in the author's analysis of the two-terminal trajectory family (ref. 19) which furnishes a typical example of such a mapping. The O-locus there was

---

*Defined as the vector of magnitude equal to the numerical eccentricity, and pointing in the direction of the lateral axis of the orbital conic (y-axis in Fig. 3).

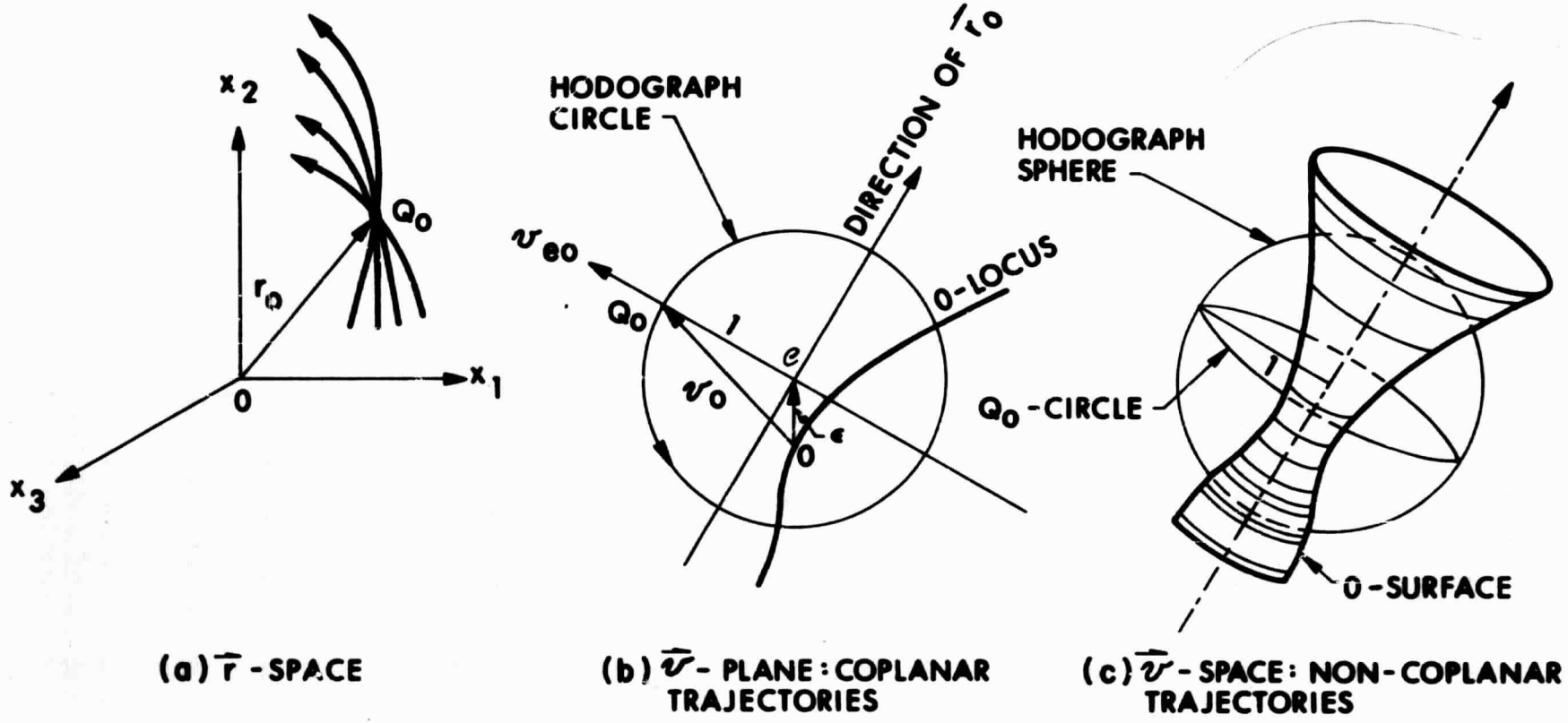

Figure 5.- The Co-terminal Keplerian Trajectory Family and Its Normalized Hodograph Image

found to be a straight line, as depicted in Fig. 6 and many interesting characteristics of the two-terminal family were derived from such linear locus. The results are contained in ref. 19. Simple O-loci have also been found for other trajectory families. Furthermore, there are cases where the normalized hodographic mapping not only simplifies the analysis, but also leads directly to the solution of the problem by the method of loci. A comprehensive presentation of the principles underlying such a mapping and its many applications cannot be incorporated here; it will be given in a separate report.

Finally, it should be mentioned that the normalized mapping may also be applied to the polar hodograph wherein the reference frame is non-inertial. The hodograph for all Keplerian orbits will then be mapped onto concentric circles all located on the V_θ-axis at a unit distance from the origin, each with a radius equal to its numerical eccentricity. In fact, the normalized polar hodograph was introduced prior to the normalized Hamiltonian hodograph outlined above. It first appeared in Boksenbom's report ref. 6 although he did not refer it as a hodographic representation. At about the same time, it was introduced as the non-dimensional special hodograph in ref. (7). Correlation between the Keplerian orbits and their normalized polar hodographs is found in refs. (7) and (10). Many examples concerning its applications are found in refs. (7) and (9). So far as the treatment of trajectory families is concerned, the normalized mapping in the inertial velocity space, as evolved from the Hamiltonian version seems preferable. However, the normalized hodograph of the polar version is found to be suitable for other classes of trajectory problems. Thus, further development of the method of normalized hodographic mapping in both versions may be desirable.

THE CONSTRAINING HODOGRAPH AND TRAJECTORY OPTIMIZATION

Problems of trajectory optimization by using impulsive thrust can be most naturally analyzed in the velocity space, since the impulsive velocity change is represented by a straight line segment there. In particular, the minimal fuel impulsive maneuver, which requires the

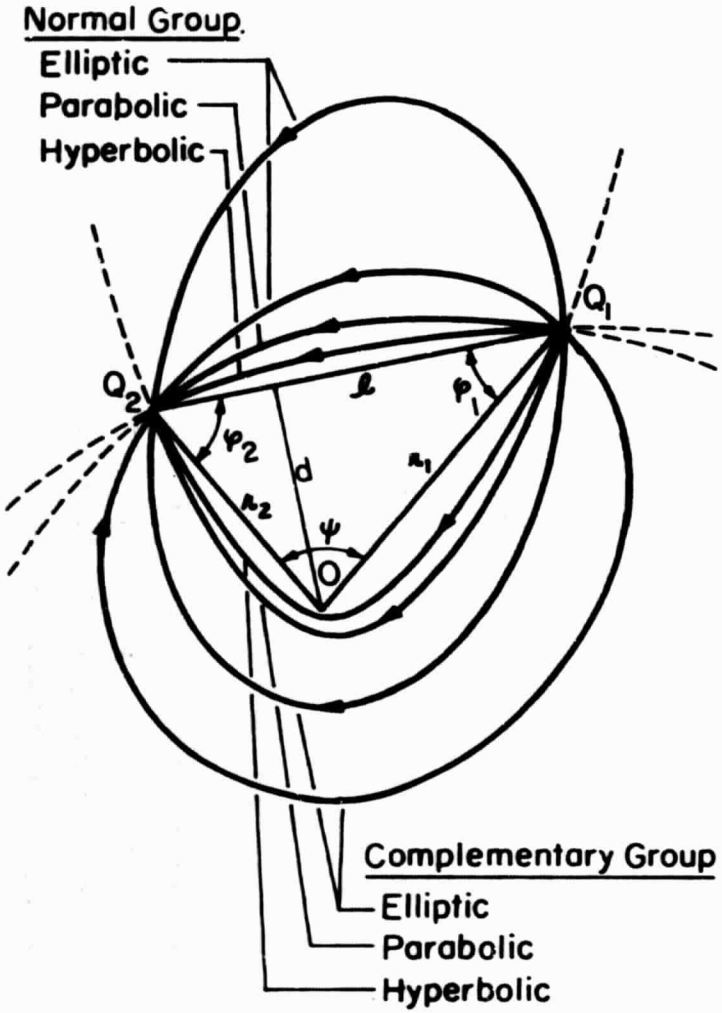

(a) $\vec{r}$ Plane

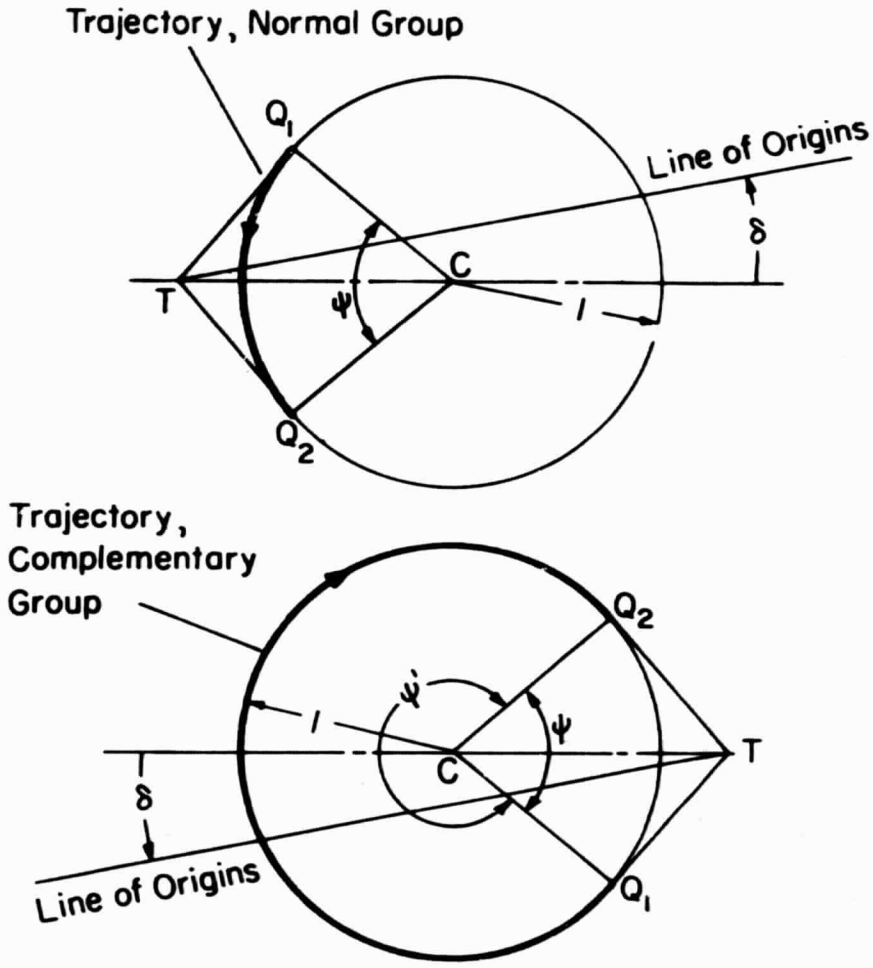

(b) $\vec{v}$ Plane

Figure 6.- The Two-Terminal Trajectory Family and Its Normalized Hodograph Image

minimization of the characteristic velocity $\sum_{i=1}^{N} |\Delta\vec{V}_i|$ always reduces to a problem of minimum sum of distances in the $\vec{V}$-space. In this connection, the concept of constraining hodograph is useful. For a family of trajectories all passing through one common terminal point Q in the $\vec{r}$-space, a constraining hodograph is the locus of the tip of the velocity vector at Q along various trajectories of the family. Such a hodograph is in a slightly different sense as that visualized by Möbius and Hamilton; and is especially useful in handling the minimal characteristic velocity problem. The conditions under which the optimization is made usually set certain constraints on the velocity vector at Q, and such constraints will appear in the form of a constraining hodograph in the $\vec{V}$-space. Since, in general, a Keplerian trajectory is uniquely determined by a position vector and the corresponding velocity vector, associated with each point on the constraining hodograph there is a unique Keplerian trajectory of the family, and vice versa. Thus, like the normalized hodographic mapping, it is again one-to-one, except possibly at certain singular points. In fact, for the same coterminal family under same constraints, the constraining hodograph in the $\vec{V}$-space is the counterpart of the normalized hodograph in the $\vec{v}$-space. The former usually has a more complicated geometry than the latter. However, the constraining hodograph has the advantage of showing all the velocity vectors in the same scale, while a normalized one does not. This advantage makes it more suitable for the minimal characteristic velocity problem wherein the magnitudes of various velocity-increments are to be compared.

It is evident that, once the constraining hodograph is mapped, the velocity-increment required to change impulsively from a given orbit to a new orbit satisfying the constraint of the problem is simply given by $\overrightarrow{Q_oQ} = \overrightarrow{\Delta V}$, where Q is a point on the constraining hodograph, and Q_o is defined by the terminal velocity on the initial orbit (Fig. 7). Thus, in a single-impulse maneuver, the problem becomes the classical geodesic problem with moving boundary; under fixed terminal conditions, the minimization of ΔV implies the orthogonality condition

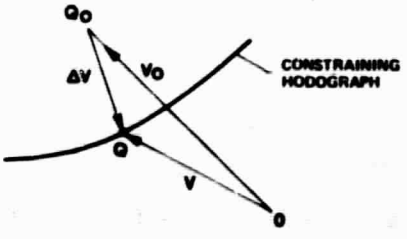

Figure 7.-The Constraining Hodograph and Impulsive Change of Orbit

$$\overrightarrow{\Delta V} \cdot \overrightarrow{dV} = 0 \qquad (30)$$

where $d\vec{V}$ is to be taken along the constraining hodograph. Equation (30) provides the analytic condition for an internal extremuim of $\vec{V}$ if it exists, and its solution gives the solution of the problem. Such an approach was first adopted by Stark (ref. 8), and later by the author (ref. 21) in the solution of the two-terminal, single impulse orbital transfer problem, where the constraining hodograph is found to be a hyperbola, and Eq (30) yields, in this case, a quartic polynomial equation in a single variable. The solution can also be obtained by constructing the normal to the constraining hodograph. In a multi-impulse maneuver, there is, in general, a constraining hodograph at each point where the impulse is applied, and the orthogonality condition (30) is to be replaced by the more general condition

$$\sum_{i=1}^{n} \frac{\Delta\vec{V}_i \cdot d\vec{V}_i}{|\Delta\vec{V}_i|} = 0 \qquad (31)$$

The application of this condition to the problem of two-terminal, two-impulse transfer yields an octic polynominal equation (18, 28). The hodograph geometry becomes quite complicated, and solutions can no longer be obtained by simple geometric construction except in special cases; however, the geometric approach in the velocity space in the light of the constraining hodograph is still profitable, as it not only enables one to obtain some geometric insight into the analytic condition expressed by Eq (31), but also helps to locate the realistic optimal solution for the problem by avoiding all the extraneous roots, the maximal solution, the unrealistic optima, etc., whatever may be present in the solution of the octic equation, and thereby reducing the time and labor of numerical computation. Such details are found in ref. 28. It is worth mentioning that, in the particular case of 180° transfer, coplanar or non-coplanar, the hodograph analysis yields a simple optimal law of equi-slope of velocity-increments for the two-impulse maneuver, and thereby leads to an analytic solution in closed form for the problem (ref. 30).

In optimal maneuver problems using continuous thrust, analyses in the acceleration space are advisable, and the use of the acceleration

hodograph in addition to the velocity hodograph may be needed. Initial studies on this subject are found in Altman's work in which the potentialities of the hodograph approach in the acceleration space are explored (ref. 22). It seems that much analytic ground and practical techniques are yet to be developed before such an approach can be effectively applied to the solution of powered trajectory problems.

ORBITAL HODOGRAPHS IN ROTATING COORDINATES

As we noted earlier, Hamilton's Law of Circular Hodograph does not hold in general in a non-inertial reference frame. However, the fundamental concepts and formulas in Table I, Section II may apply to a non-inertial frame with proper re-interpretation of the sympols $\vec{r}$, $\vec{v}$, and $\vec{F}$. In the following, the hodographic mapping of Kepler orbits in a rotating coordinate system will be introduced. The system (X_R, Y_R) is assumed to be rotating at a uniform angular speed n_o in the plane of motion, with its origin at the field center. For convenience, we use the complex variables

$$z = re^{i\theta} \tag{32}$$

$$w = ve^{i\beta} \tag{33}$$

to represent the position and velocity of the moving particle in the apsidal coordinate system, which is fixed in the inertial space (sidereal), and similarly,

$$Z = re^{i\theta_R} \tag{34}$$

$$W = V_R e^{i\beta_R} \tag{35}$$

in the rotating (synodic) coordinate system, where the symbols θ, θ_R etc. are defined in Fig. 8. The orbits in the z- and Z- planes are the absolute (or sidereal) and the relative (or synodic) orbits respectively; and the corresponding ones in the w- and W-planes are the absolute (or sidereal) and relative (or synodic) hodographs respectively. Assuming the two coordinate systems coinciding at t = 0, the transformation equation between these two systems are

$$Z = ze^{-in_o t} \tag{36}$$

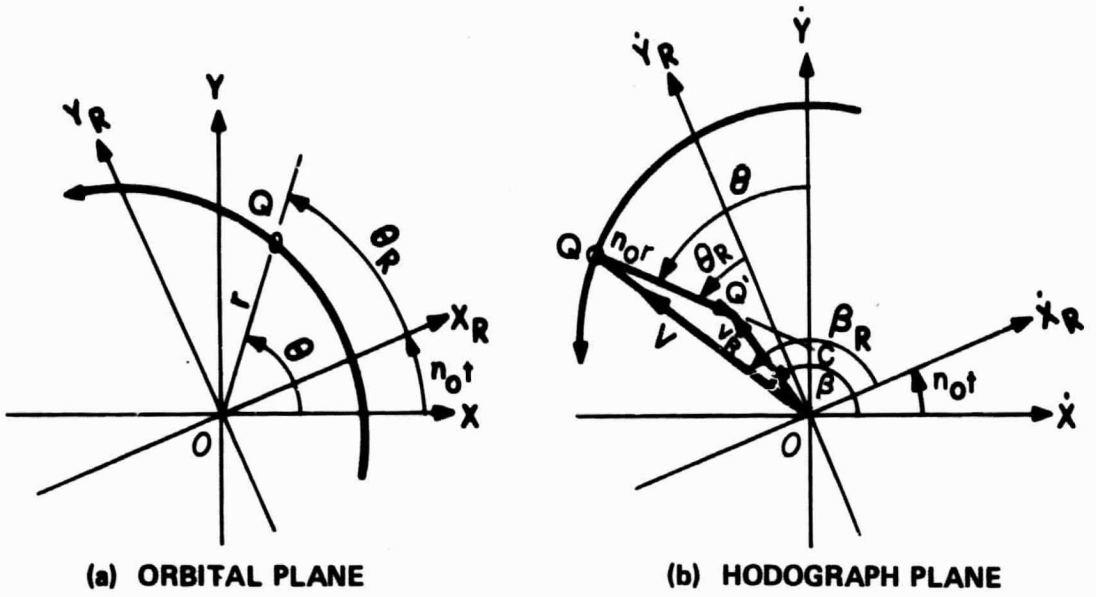

Figure 8.- Fixed and Rotating Coordinate Systems for Orbital Motion

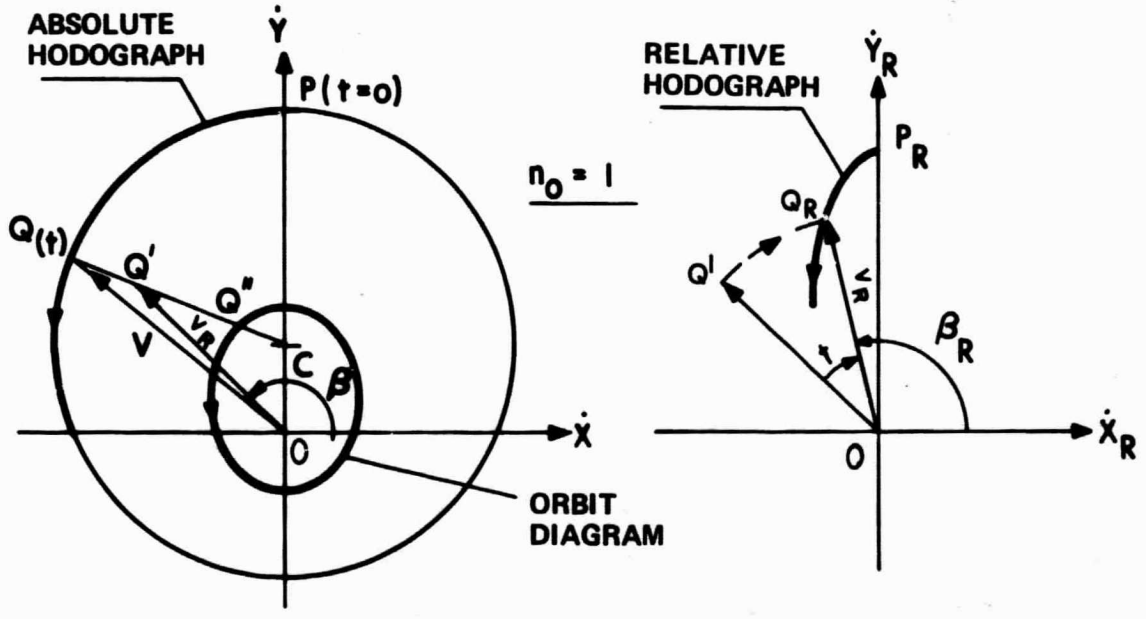

Figure 9.- Graphic Mapping of the Orbital Hodograph: From Sidereal System to Synodic System

$$W = (w - in_o re^{i\theta})\ e^{-in_o t} \tag{37}$$

For a Kepler orbit of angular momentum h and eccentricity ε, we may show that

$$V_R = \frac{\left\{\left[V^2 - 2n_o h\right]\left[V^2 + \frac{\mu^2}{h^2}(1-\varepsilon^2)\right]^2 + 4\mu^2 n_o^2\right\}^{1/2}}{V^2 + \frac{\mu^2}{h^2}(1-\varepsilon^2)} \tag{38}$$

$$\beta_R = \tan^{-1}\left[\frac{\left[\varepsilon \sin\beta + \sqrt{1-\varepsilon^2\cos^2\beta}\right]\left[\varepsilon \sin\beta\sqrt{1-\varepsilon^2\cos^2\beta} - \varepsilon^2\cos^2\beta + 1 - \frac{n_o h^3}{\mu^2}\right]\sin\left(\beta - n_o t\right) + \frac{n_o h^3}{\mu^2}\varepsilon\cos n_o t}{\left[\varepsilon \sin\beta + \sqrt{1-\varepsilon^2\cos^2\beta}\right]\left[\varepsilon \sin\beta\sqrt{1-\varepsilon^2\cos^2\beta} - \varepsilon^2\cos^2\beta + 1 - \frac{n_o h^3}{\mu^2}\right]\cos\left(\beta - n_o t\right) + \frac{n_o h^3}{\mu^2}\varepsilon\sin n_o t}\right] \tag{39}$$

where h is considered positive if the rotational sense of the orbit agrees with that of the rotating coordinate system, as viewed from a fixed system; otherwise, it is considered negative. These transformation formulas (38, 39) look cumbersome; however, the hodographic mapping may be effected by simple geometrical constructions, which follow directly from Eq (37), as follows:

(1) Choose units such that $n_0 = 1$, and superimpose the orbit diagram on the circular hodograph (Hamiltonian version) such that the occupied focus coincides with the center of the hodograph circle, and its apsidal axis coincides with the y-axis (see Fig. 9).

(2) Attach a time scale to the circumference of the hodograph circle in accordance with the appropriate Kepler equation.

(3) Consider an arbitrary orbital point Q on the hodograph circle, and connect Q and C, intersecting the orbital conic at Q'.

(4) On CQ or its extension, according as h is positive or negative lay off QQ' = CQ", to obtain the vector QQ'.

(5) Rotating QQ' through an angle -t (the time corresponding to Q) to transfer the point Q' to Q_R, then we have $QQ_R = \vec{V}_R$, thus completing the mapping for the orbital point 0 (see Fig. 9). The entire orbit may thus be mapped point-wise.

It is important to note that an essential difference between an absolute hodograph and a relative hodograph is that while the tangent to the former points the direction of the external force, that to the latter points the direction of the apparent force, which is the vector difference between the external force and the Coriolis and centrifugal forces. Thus on the absolute and relative hodographs, one finds readily the directional deviation of the apparent force from the local gravity force.

The foregoing transformation formulas (38, 39), and geometric constructions apply regardless of the eccentricity of the orbital conics, except that, in step 2 under geometric construction, the Kepler equation pertinent to the particular type of the conic has to be used. As an example, a typical Kepler elipse and its hodograph in both the sidereal system and the synodic system are shown in Fig. 10. It is seen that the orbital hodograph in the synodic system is much more complicated than the circular hodograph in the sidereal system. The introduction of such seemingly unnecessary complications is motivated by the fact that Kepler problem is the limiting case of a restricted three-body problem when one of the primaries approaches zero mass, and in treating the restricted three-body problem, the use of the synodic system is superior and prevailing. Thus, by referring to such a coordinate system, the information obtained for the two-body problem may be directly compared with that for a three-body problem. Literature on synodic Kepler orbits is rather scarce. An inclusive treatment of this subject is found in Hoelker and Winston's recent work (ref. 27), in which extensive comparisons of a class of Earth-Moon orbits with a class of Rotating Kepler orbits, both in the position space, were made. The present section briefly illustrates what can be done in the velocity space. It is hoped that such a synodic hodograph may provide additional basis for such comparitive studies.

THE OSCULATING HODOGRAPH AND ORBITAL PERTURBATION

In a gravity field with the presence of perturbing forces, the Hamiltonian circular hodograph can no longer apply, even in an inertial reference frame, and the analysis may proceed on the basis of the

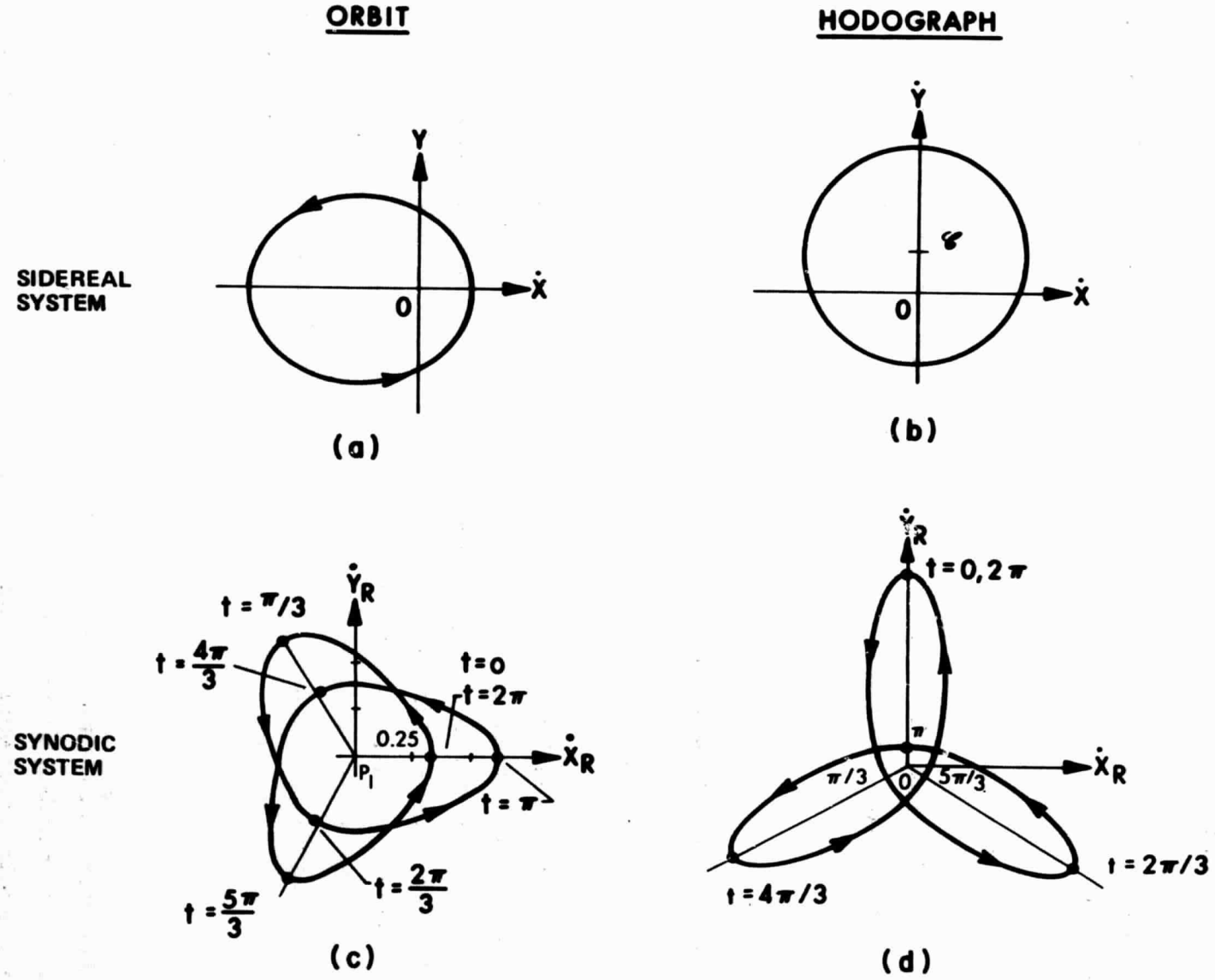

Figure 10.- The Elliptic Orbit and Its Hodograph Image in Sidereal and Synodic Systems: $\mu = 1$, $n_0 = 1$, $n = 3$, $\varepsilon = 0.3$ (Fig. (c) Taken from Szebehely's Text, Ref. 23, p. 414; Fig. (d) Not Drawn to Scale)

general formulas presented in Section II. However, in many perturbation problems, the classical concept of osculating conics is profitable, and it can be extended to the velocity space. Following such a concept, the instantaneous vectors $\vec{r}$ and $\vec{V}$ define an osculating conic in the $\vec{r}$-space, and a corresponding osculating circular hodograph in the $\vec{V}$-space, characterized by the two parameters,

$$R = \frac{\mu}{h} , \quad \vec{C} = \vec{V} - R \frac{\vec{h}}{h} \times \frac{\vec{r}}{r} \tag{40}$$

where $\vec{h} = (\vec{r} \times \vec{V})$ is the angular momentum vector as defined before. Eliminating $\vec{h}$ between Eqs. (40) by introducing the vector $\vec{R}$, defined by

$$\frac{\vec{R}}{R} = \frac{\vec{h}}{h} \tag{41}$$

reduces the second of Eqs. (40) to

$$\vec{V} = \vec{C} + \vec{R} \times \frac{\vec{r}}{r} \tag{42}$$

which is the form used by Altman (ref. 29) with slightly different notations. Without perturbation, the motion is Keplerian, and both vectors $\vec{C}$ and $\vec{R}$ are constants, in accordance with the invariant velocity components theorem (see Section III). When perturbations are present, $\vec{C}$ and $\vec{R}$ may then be regarded as two osculating elements (see Fig. 11). In contrast with the usual scalar Keplerian elements, they are vectors, and have the dimension of velocity. They will be referred to as the kinematic osculating elements. It is important to note that $\vec{C}$ and $\vec{R}$ are related by

$$\vec{C} \cdot \vec{R} = 0 \tag{43}$$

Thus, of the six components of $\vec{C}$ and $\vec{R}$, only five of them are independent. In other words, the two vectorial elements $\vec{C}$ and $\vec{R}$ provide five independent scalar elements, which, together with the epoch t, determine completely a set of six osculating elements for the perturbed orbit. The usual Keplerian, Jacobi, and Delaunay sets of elliptic elements are related to this vector pair $\vec{C}$ and $\vec{R}$ as summarized in Table 2. Similar

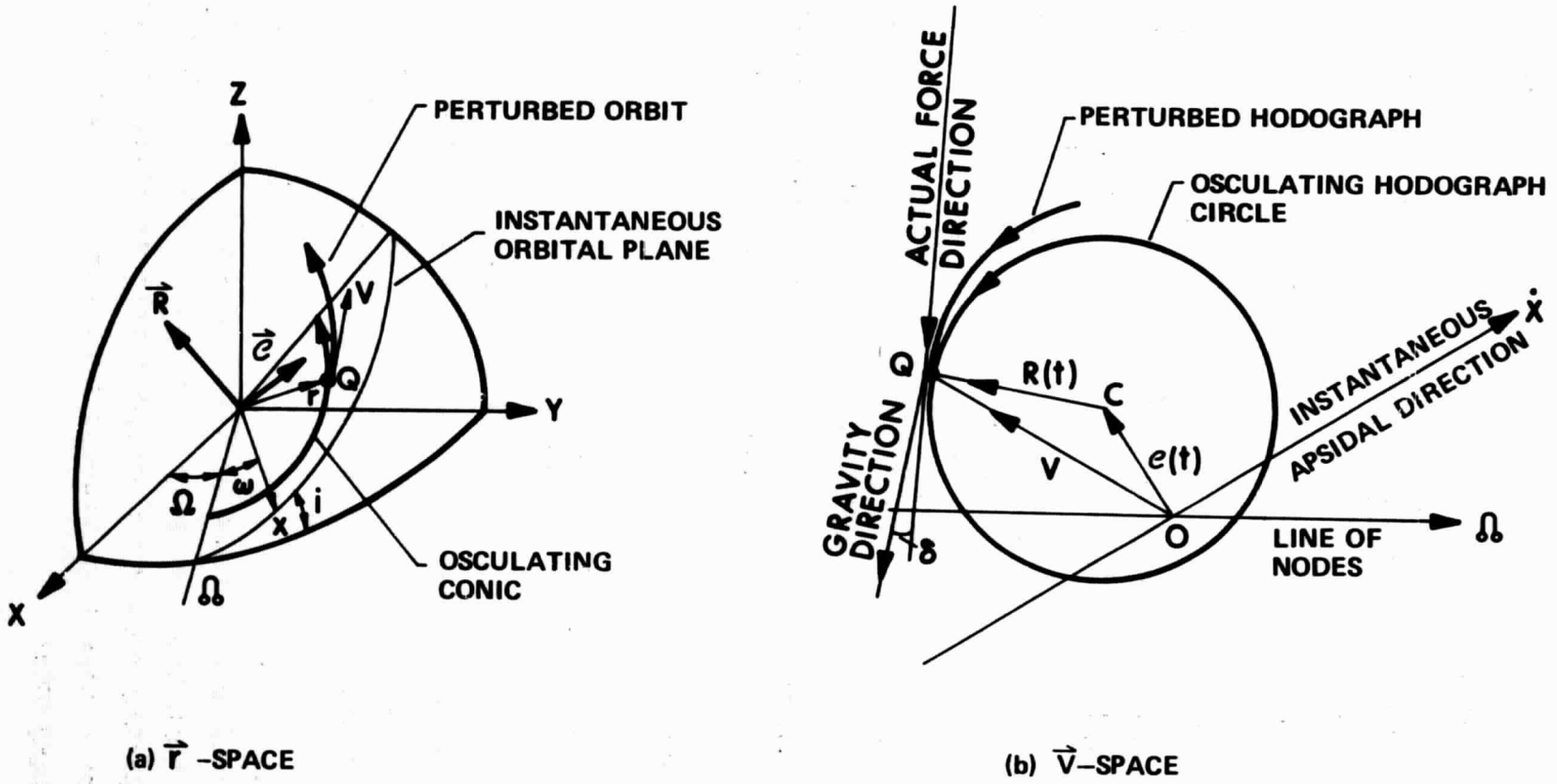

Figure 11.- The Perturbed Orbit and the Osculating Conic and Their Hodograph Images

relations may be written for the modified Delaunay set of elements and the Poincare and his modified sets.

TABLE II

ELLIPTIC ELEMENTS IN TERMS OF THE KINEMATIC PARAMETERS $\vec{C}$ AND $\vec{R}$ ($R>C$)

	Keplerian	Jacobi	Delaunay
q_1	$a = \frac{\mu}{R^2-C^2}$	$k = \frac{1}{2}(R^2-C^2)$	$\sqrt{\mu a} = \frac{\mu}{\sqrt{R^2-C^2}}$
q_2	$e = \frac{C}{R}$	$h = \frac{\mu}{R}$	
q_3	$i = \cos^{-1}\frac{R_z}{R}$	$h_z = \mu\frac{R_z}{R}$	
P_1	$-T = \frac{\mu}{\left[R^2-C^2\right]^{3/2}}\left\{\sin^{-1}\left[\frac{1}{C}\sqrt{C^2-\left(\frac{\mu}{rR}-R\right)^2}\right] - \frac{1}{R}\sqrt{C^2-\left(\frac{\mu}{rR}-R\right)^2}\right\}-t$		$n(t-T) = \sin^{-1}\left[\frac{1}{C}\sqrt{C^2-\left(\frac{\mu}{rR}-R\right)^2}\right] - \frac{1}{R}\sqrt{C^2-\left(\frac{\mu}{rR}-R\right)^2}$
P_2	$\omega = \tan^{-1}\frac{C_xR_y - C_yR_x}{C_zR}$		
P_3	$\Omega = \tan^{-1}\frac{R_x}{-R_y}$		

Note: q_1 and P_1 ($i=1,2,3$) are canonical conjugates except for Keplerian elements

Explicit expressions for the rates of change of the kinematic osculating elements in terms of the disturbing forces are found as follows:

$$\dot{\vec{R}} = -\frac{rR^2}{\mu}\left(F_h\vec{e}_\theta + F_\theta\vec{e}_h\right) \tag{44}$$

$$\dot{\vec{C}} = F_r\vec{e}_r + \left(1+\frac{rR^2}{\mu}\right)F_\theta\vec{e}_\theta + \left(1-\frac{rR^2}{\mu}\right)F_h\vec{e}_h \tag{45}$$

where F_r, F_θ and F_h are the disturbing force components in the local orbital polar frame of reference. The rates of change of other elements may be readily related to $\vec{C}$ and $\vec{R}$ through the equations of Table 2. A glance at Eqs. (44, 45) enables one to infer immediately that:

> The osculating hodograph circle will remain fixed in size, and the plane of motion will be fixed in the inertial space, if the perturbing force is purely radial; however, the location of the center of the hodograph circle as given by the vector element $\vec{C}$ will vary under the presence of any disturbing force component.

No extensive analysis nor discussions can be elaborated within the limited scope here. The significance of these kinematic elements have been noticed by Cronin,[14] Schwartz,[14] Pohle,[15] Altman,[29] and others, but literature on their practical applications to trajectory analysis is scarce. Preliminary studies in this direction are found in Ref. 14, 15, and 29. It seems much analytical work is yet to be done in order to use these kinematic osculating elements as the principal parameters in the analysis and predication of perturbed orbits or trajectories.

Finally, as a word of caution, the concept of the osculating circular hodograph should not be confused with that of the osculating circle of the hodograph.* The former is in the instantaneous plane of $\vec{r}$ and $\vec{V}$, while the latter is in the osculating plane of the $\vec{V}$-trajectory, defined by $\vec{e}_T$ and $\vec{e}_N$ (see Section II.) These two planes do not coincide unless the motion is planar; and even when they do, the radius of the hodograph circle and that of the osculating circle of the hodograph, which is the radius of curvature of the $\vec{V}$-trajectory will not be equal unless the field is Newtonian and free from perturbations. The concepts of the osculating conic and its corresponding osculating hodograph circle are most useful when the field is Newtonian, and the perturbation is small; while the concept of the osculating circle of the hodograph and the related formulas in Section II, with reference to the Frenet frames in the $\vec{r}$- and $\vec{V}$-spaces are generally applicable in any non-inverse-square or non-central force field.

---

*Mathematically speaking, "osculating" implies contact of order at least 2. While the term "osculating circle of the hodograph" is correct in this sense, the terms "osculating conic" and "osculating circular hodograph" are generally not. However, to conform to the classic literature on orbital purturbation, the conventional term "osculating conic" is retained here, and the term "osculating circular hodograph" is understood to mean the hodograph corresponding to the osculating conic.

EXTENSION OF HODOGRAPHIC MAPPING TO HIGHER ORDER VECTOR SPACES

So far the discussions have been confined to velocity hodographs. Theoretically, there is no limitation on the concept of hodograph as to its applicability to the vector spaces higher than the velocity space. In general, we may define an nth order hodograph as the trajectory in the $\vec{r}^{(n)}$ - space, where the superscript (n) denotes the nth time derivative of $\vec{r}$. In particular, we have

$n = 0$: $\vec{r}$ - space (position)

$n = 1$: $\dot{\vec{r}}$ - space (velocity)

$n = 2$: $\ddot{\vec{r}}$ - space (acceleration)

$n = 3$: $\dddot{\vec{r}}$ - space (jerk)

These are the state-spaces as called by Altman, and his poineer work in this direction is found in Ref. 29. The fundamental concepts and formulation presented in Section II provide a logical basis for such extensions, and all formulas presented therein for the position and velocity spaces may be applied to the nth order space by replacing the vectors $\vec{r}$, $\vec{V}$, and $\vec{F}/m$ by $\vec{r}^{(n-1)}$, $\vec{r}^{(n)}$ and $\vec{r}^{(n+1)}$ respectively. In principle, n is not necessarily restricted to a positive integer. For example, with the understanding that the symbol $r^{(-1)}$ stands for $\int^{t}\vec{r}(t)dt$, we may define an inverse hodograph as the trajectory in the $r^{(-1)}$ - space; and, more generally, we may speak of a $r^{(n-1)}$ - trajectory as the inverse hodograph of the $r^{(n)}$ - trajectory. The possible application of the acceleration hodograph has been mentioned in Section V in connection with trajectory optimization. The orbital acceleration hodograph for Kepler motion has been found by Altman to be a form of Pascal's limacon.[17] So far it seems no analytical work has been done beyond the acceleration hodograph in an inverse-square field. A rigorous treatment for the general nth order hodograph, including all position, velocity, acceleration, jerk spaces, etc., as its special cases, from both analytic and geometric points of view, would put the hodograph theory on a firm foundation, and thereby enlarge its field of application to a great variety of problems in space-flight.

FINAL REMARKS

As contrasted with the classical methods in Hamiltonian Mechanics, including the canonical transformation and the Hamilton-Jacobi equation, which deals with a 2n-dimensional phase space in the n pairs of the generalized conjugate coordinates, the hodograph method is a direct approach in the velocity space, with possible inclusion of the acceleration space and other higher order spaces as required. In fact, the velocity space may be regarded as the linear momentum space for a constant mass, and, together with the position space, it provides an initial set of canonical coordinates for the basic Hamiltonian formulation. In as much as the result of a formalistic solution of the Hamilton-Jacobi equation must be finally interpreted in terms of the position, velocity, and possibly acceleration spaces, etc., the direct approach in these spaces by the hodograph method is advisable whenever it is feasible.

It is generally recognized that the methods of classical Haniltonian mechanics are highly analytic, while the hodographic mapping is highly geometric. However, it is worth noting that, in classic calculus of variation, which is the basis of the celebrated Hamilton's principle, the Euler-Lagrange equation defines essentially the curvature of the extremal; and that many standard problems in calculus of variations are geometric in nature, notably the geodesic problem and the isoperimetrical problem. Thus, it would be no surprise to see that a trajectory problem, governed by the Hamiltonian equations of motion, reduces to a standard geometrical problem through hodographic mapping, and that an optimal law deduced from such hodograph analysis resembles the Fermat's law in optics, as both are the law of shortest path from the geometric point of view (see Section V and Ref. 28, 30). However, while the reduction of a dynamic problem to a geometric problem by such a mapping may give a new look of the problem, and may provide some geometrical insight into the situation from the geometry of the hodograph image of the dynamic system, it does not usually yield the solution directly; and to find the solution of the problem one often needs to solve the Eular-Lagrange equation or the Hamilton-Jacobi equation. Thus the analytic approach of the classic methods and the geometric approach of the hodographic

mapping are complementary to each other, and an ingenious combination of them may be needed in a complicated trajectory problem.

As we know, the classic methods in Hamiltonian Mechanics have been well developed over the past hundred years, and found vast applications in many branches of physics, from the classic dynamics to modern space flight. The recent work by Miner, Tapley, Powers, and Andrus[25,26] fully illustrates how the classic techniques of calculus of variation, canonical transformation, the Hamilton-Jacobi equation, and the variation of orbital parameters could be combined to apply to the current problems of space flight, like the low-thrust trajectory and the optimal lunar trajectories. On the other hand, the hodograph method, also originated by Hamilton, has been virtually unnoticed, until a decade ago, despite Hamilton's brilliant pioneer work, as mentioned in the Introduction; hence only limited applications have been effected, and many possibilities are untried. The joint use of the hodographic mapping with the classic methods is even rarer, though Contensou's work on optimal trajectories[13] appears to be in this direction. At the present stage the Hamiltonian hodograph and its many modern developments as introduced in Sections III through VII, seem best suited in the area of two-body problem, the global analysis of families of Kepler orbits, and the impulsive orbital maneuver, with possible applications in the perturbation problem, the restricted three-body problem, and others. To further develop the art of hodographic mapping, to build its theoretical foundation, to perfect its techniques, and to enlarge its field of application in order that it may become a true partner of the classical methods in coping with the challenge of the new trajectory problems as well as many other dynamic problems encountered in modern space-flight, much theoretical and practical work has yet to be done.

REFERENCES

1. Möbius, A. F.: Die Elemente der Mechanik des Himmels, Weidmannsche Buchhandlung, Leipzig, 1843, pp. 28-59 (Gesammelte Werke, vol. IV, Verlag von S. Hirzel, Leipzig, 1887).

2. Hamilton, Sir William R.: The Hodograph, or a New Method of Expressing in Symbolical Language the Newtonian Law of Attraction, Proc. Roy. Irish Acad. vol. III, 1845-47, pp. 344-353 (read Dec. 1846).

3. Hamilton, Sir William R.: Elements of Quaternions, vol. I, 1899, p. 99, vol. II, 1901, pp. 29, 298-320, Longmans Green and Co., London.

4. Whittaker, E. T.: A Treatise on the Analytical Dynamics of Particles and Rigid Bodies, Cambridge Univ. Press, 1937, 4th ed., p. 89.

5. Altman, S. P.: Orbital Transfer for Satellites, Fourth Ballistic Missile and Space Technology Symposium, Aug. 1959, Proc., Pergamon Press, New York, 1961, pp. 132-144.

6. Boksenbom, A.S.: Graphical Trajectory Analysis, NASA TN D-64, Dec. 1959.

7. Sun, F. T.: A Special Hodograph for Orbital Motion, 2nd International Symposium on Rockets and Astronautics, Tokyo, May 1960, Proc., Yokendo Bunkyo-Ku, Tokyo, 1961, pp. 163-189.

8. Stark, H. M.: Optimum Trajectories Between Two Terminals in Space, ARS J., Feb. 1961, pp. 261-263.

9. Sun, F. T.: Some Applications of the Special Hodograph for Orbital Motion, 3rd International Symposium on Rockets and Astronautics, Tokyo, Aug. 1961, Proc., Yokendo Bunky-Ku Tokyo, 1962, pp. 381-396.

10. Sun, F. T.: On the Hodograph Method for Solution of Orbit Problems, XIIth International Astronautical Congress, Washington, D.C., Oct. 1961, Proc. vol. II, pp. 879-915, Academic Press, 1963.

11. Altman, S. P., and Pistiner, J. S.: Polar Hodograph for Ballistic Missile Trajectories, ARS J., vol. 31, no. 11, Nov. 1961.

12. Altman, S. P., and Pistiner, J. S.: Hodograph Transformation and Mapping of the Orbital Conics, ARS J. vol. 32, no. 7, July 1962.

13. Contensou, P.: Etude Theorique des Trajectories Optimals Danes on Champ de Gravition. Application au cas d'un centre d'attraction unique, Astronautic Acta, vol. VIII/FASC 2-3, 1962.

14. Cronin, J. L. and Schwartz, R. E.: Invariant Two-body Velocity Components, J. Aerospace Sci. 29, 1384-85, 1962.

15. Pohle, R. B.: Invariant Components of Motion in Inverse-Square Force Field, AIAA J. vol. 1, no. 4, April 1963.

16. Desek, Rudolf, Invariant Two-Body Velocity Components and the Hodograph, AIAA J., vol. 1, no. 7, July 1963.

17. United Aircraft Corporate Systems Center, Research Study on the Acceleration Hodograph and Its Application to Space Trajectory Analysis, NASA CR-19, Sept. 1963.

18. Altman, S. P. and Pistiner, J. S.: Analysis of the Orbital Transfer Problem in Three-Dimensional Space, Progress in Astronautics and Aeronautics, vol. 14, Academic Press, New York, 1964, pp. 627-654.

19. Sun, F. T.: Hodograph Analysis of the Free-Flight Trajectories Between Two Arbitrary Terminal Points, NASA CR-153, Jan. 1965.

20. Altman, S. P.: Orbital Hodograph Analysis, AAS Science and Technology Series, vol. 3, Western Periodicals, 1965.

21. Sun, F. T.: On the Optimum Transfer Between Two Terminal Points with Minimum Initial Impulse under an Arbitrary Initial Velocity Vector, NASA CR-622, Washington D.C., Nov. 1966.

22. Altman, S. P.: Derivation of Analytical Methods Which Give Rapid Convergence to the Solution of Optimized Trajectories, GE MSD Reports DIN 67SD4315, 4318, 4304, 4300, June 1967.

23. Szebehely, V.: Theory of Orbits, Academic Press, 1967, pp. 402-417.

24. Eades, J. B., Jr.: Orbit Information Derived from Its Hodograph, Report No. X-643-68-264, Goddard Space Flight Center, NASA, July 1968.

25. Miner, W. E., Tapley, B. D., and Powers, W. F.: The Hamilton-Jacobi Method Applied to the Low-Thrust Trajectory Problem, XVIII International Astronautical Congress, Belgrade, 1967, Pergamon Press, 1968, pp. 293-305.

26. Miner, W. E., and Andrus, J. F.: Necessary Conditions for Optimal Lunar Trajectories with Discontinuous State Variables and Intermediate Point Constraints, AIAA J. vol. 6, no. 11, Nov. 1968, pp. 2154-2159.

27. Hoelker, R. F., and Winston, B. P.: A Comparison of a Class of Earth-Moon Orbits with a Class of Rotating Kepler Orbits, NASA TN D-4903, Washington, D.C., Nov. 1968.

28. Sun, F. T.: Analysis of the Optimum Two-Impulse Orbital Transfer under Arbitrary Terminal Conditions, AIAA Guidance, Control, and Flight Dynamics Conference, Aug. 1967, AIAA J. vol. 6, no. 11, Nov. 1968.

29. Altman, S. P.: Application of State Space Transformation Theory to Orbit Determination and Prediction, AAS/AIAA Astrodynamics Specialist Conference, Jackson, Wyoming, Sept. 1968, AAS Paper No. 68-111.

30. Sun, F. T.: Analytic Solution for Optimal Two-Impulse 180° Transfer Between Noncoplanar Orbits and the Optimal Orientation of the Transfer Plane, AAS/AIAA Astrodynamics Specialist Conference, Jackson, Wyoming, Sept. 1968, AAS Paper No. 68-093.